Feasibility of Surfactant-Free Supported Emulsion Liquid Membrane Extraction

Shih-Yao B. Hu, Jin Li, and John M. Wiencek*
The University of Iowa
Department of Chemical and Biochemical Engineering

Running Title: Surfactant-Free SELM Extraction

*Corresponding Author
John M. Wiencek
4122 Seamans Center
Iowa City, IA 52242-1527
wiencek@engineering.uiowa.edu
Voice: (319) 353-2377
FAX: (319) 335-1415

Abstract

Supported emulsion liquid membrane (SELM) is an effective means to conduct liquid-liquid extraction. SELM extraction is particularly attractive for separation tasks in the microgravity environment where density difference between the solvent and the internal phase of the emulsion is inconsequential and a stable dispersion can be maintained without surfactant. In this research, dispersed two-phase flow in SELM extraction is modeled using the Lagrangian method. The results show that SELM extraction process in the microgravity environment can be simulated on earth by matching the density of the solvent and the stripping phase. Feasibility of surfactant-free SELM (SFSELM) extraction is assessed by studying the coalescence behavior of the internal phase in the absence of the surfactant. Although the contacting area between the solvent and the internal phase in SFSELM extraction is significantly less than the area provided by regular emulsion due to drop coalescence, it is comparable to the area provided by a typical hollow-fiber membrane. Thus, the stripping process is highly unlikely to become the rate-limiting step in SFSELM extraction. SFSELM remains an effective way to achieve simultaneous extraction and stripping and is able to eliminate the equilibrium limitation in the typical solvent extraction processes. The SFSELM design is similar to the supported liquid membrane design in some aspects.

Keywords: extraction, hollow fiber, emulsion, propionic acid, microgravity, liquid membrane, surfactant.

Introduction

Supported emulsion liquid membrane (SELM) extraction is an effective technique to conduct liquid-liquid extraction. In a typical SELM extraction, a water-in-oil emulsion liquid membrane (ELM) is first formulated by dispersing an aqueous solution into an organic solvent. The aqueous phase, stabilized by surfactant, forms numerous micro-droplets within the continuous, organic phase. The emulsion is then brought into contact with an aqueous feed stream via a microporous hollow-fiber membrane. The solute dissolves into the organic solvent, then is transported to the surface of the internal aqueous droplets, and finally partitions into the internal aqueous droplets. Because of the stripping mechanism provided by the internal phase, the solute concentration in the organic solvent is maintained at a low level and a high extraction efficiency can be sustained for a long period of time. The SELM design inherits all the benefits of membrane-based extraction, namely dispersion-free operation and easy scale-up, while eliminating the equilibrium limitation of common extraction process. SELM also minimizes the leakage and swelling problems associated with dispersive ELM extractions. SELM has been successfully used for the extraction of heavy metals and organics (1,2,3).

A tradeoff of SELM's high extraction capacity is that the ELM must be demulsified to recover the product. Due to density differentials between the solvent and the internal phase, surfactant is usually required to maintain a stable dispersion. Demulsification may be achieved chemically or by heat treatment (4). Electrostatic coalescence has been used extensively for the demulsification of coarse, water-in-oil emulsion industrially (5). Success has also been reported on a membrane-based demulsification method (6).

Recently, the authors proposed the possibility of surfactant-free SELM (SFSELM) extraction in the microgravity environment (7). Because the density differential will not result in

phase segregation in the microgravity environment, a stable dispersion of the stripping phase within the solvent may be maintained even without surfactant. The benefit of SELM can be realized without the drawback of the demulsification process. SFSELM extraction provides an efficient way for media recycle and can have significant impact on the sustainability of bioreactors aboard spacecrafts. High ground-to-orbit launch costs as well as the utility costs of refrigeration for storage makes the media requirement quite substantial in space experiments. Purification and reuse of complex media are needed for long duration cell culture in outer space. On earth, media is typically discarded after a single use, which usually leads to expensive wastewater treatment afterwards; therefore, it is also beneficial to recycle media on earth as well. SFSELM extraction on earth is also possible if the densities of the solvent and the stripping phase are closely matched.

In this research, the feasibility of SFSELM extraction is assessed. The research consists of two part. The first part is a proof-of-concept study that deals with the droplet trajectory in SFSELM extraction under various conditions. Besides stabilizing the immiscible dispersion in the emulsion, the presence of surfactant also minimizes the size of the stripping phase droplets. The fine dispersion of emulsion provides enormous contacting area for the stripping step and minimizes the mass transfer resistance. The main concern of SFSELM extraction is, thus, the loss of contacting area due to the elimination of surfactant. The second part of the research studies the effect of drop coalescence on the contacting area between the solvent and the internal phase.

Effect of Density Differentials on Drop Trajectory

SFSELM is basically a dispersed two-phase system. Analogies of the fluid mechanics in SFSELM may be drawn from commonly used chemical process such as the bubble column and the fluidized bed. Various approaches have been used to model such dispersed two-phase flow systems. The most notable ones are the Eulerian method (8), the Algebraic Slip Mixture Model (ASMM) (9), and the Lagrangian method (10). The Lagrangian method allows the tracking of the trajectory of each particle and is used ihere. In the Lagrangian method, the carrier phase is treated as a continuum and is subject to the mass, momentum and energy conservation equations. The effect of the dispersed phase is coupled into these equations as source terms. Thus, the continuity equation at steady state may be written in tensor notation as

$$\frac{\partial(\rho u_j)}{\partial x_j} = \Phi^m \tag{1}$$

where ρ is the density of the continuous phase and u is the velocity of the continuous phase. Φ^m is the source term that accounts for the mass exchange between the continuous phase and the dispersed phase. The subscript j indicates the spatial coordinates; j = 1, 2 and 3 corresponds to the X, Y and Z direction respectively. Unlike in the case of bubble column reactor, mass exchange between the solvent and the stripping phase is usually insignificant in liquid-liquid SELM extraction and the source term is negligible; *i.e.* $\Phi^m = 0$. In addition, constant density may be assumed for liquid flow. The continuity equation thus reduces to

$$\frac{\partial u_j}{\partial x_j} = 0 \tag{2}$$

The equation of momentum conservation in the i direction at steady state may be written as

$$\frac{\partial}{\partial x_j}\left(\rho u_i u_j\right) = -\frac{\partial p}{\partial x_i} + \frac{\partial \tau_{ji}}{\partial x_j} + \rho g_i + \Phi_i^M \tag{3}$$

where p is the pressure and τ is the normal and shear stress and g is the gravitational acceleration. The subscript i represent the X, Y or Z direction. Φ_i^M is the source term representing momentum transfer between the carrier phase and the dispersed phase, which is typically the result of drag force. The system is assumed to be isothermal so the energy conservation equation is neglected. For Newtonian flow of constant density, equation (3) may be written as

$$\rho\left(\frac{\partial u_i}{\partial x_j} u_j\right) = -\frac{\partial p}{\partial x_i} + \mu \frac{\partial^2 u_j}{\partial x_j^2} + \rho g_i + \Phi_i^M \tag{4}$$

where μ is the viscosity of the continuous phase. As the name suggests, the trajectory of the dispersed phase is modeled using the Lagrangian approach on each droplet:

$$\frac{du_i^p}{dt} = \frac{\left(u_i - u_i^p\right)}{\lambda} + \left(\frac{\rho^p - \rho}{\rho}\right) g_i \tag{5}$$

where $u^p{}_i$ is the droplet velocity in the i direction and ρ^p is the droplet density. λ, the particle relaxation time, is defined as

$$\lambda = \frac{4\rho^p D^{p^2}}{3\mu C_D \,\mathrm{Re}^p} \tag{6}$$

where D^p is the droplet diameter, C_D is the drag coefficient and Re^p is the droplet Reynolds number ($\mathrm{Re}^p = (u\text{-}u^p)D^p\rho/\mu$). Equation (6) is a simple momentum balance based on Newton's second law of motion; the first term on the right-hand side is the drag force while the second term contains the buoyancy and gravitational forces. The impact of the droplets on the continuous phase is accounted for through the source term Φ_i^M in equation (3) and (4). When the

system is modeled numerically, the computational domain is divided into an array of small control volumes and the source term may be coupled into the each control volume by

$$\Phi_i^M(E) = \frac{1}{V_E}\sum_{k=1}^{n_E}\eta_k \int_{\delta t_k} \rho^p V^p \frac{\left(u_i - u_i^p\right)}{\lambda} dt \qquad (7)$$

where E denotes a control volume of interest, V is the size of the control volume, n_E is the number of droplets within the control volume, k denotes a certain trajectory and η_k is the number of droplets within the control volume that follow the same trajectory, V^p is the droplet volume, and δt_k is the residence time of droplets within the control volume that follow the trajectory k. A particle is monitored as soon as it is introduced into the computational domain and the trajectory of the particle may be obtained by integrating equation (5) from an initial location. An unsteady-state simulation is also possible. However, tracking of the numerous droplets and trajectories is computationally expensive and is beyond the scope of this study. The system is modeled using the commercial software package Fluent (Fluent, Inc., NH).

The simulations assume that the ELM flows through the lumen side of a hollow fiber membrane. The conditions used were similar to previous experimental studies (1,7). Specifically, the fiber lumen has a length of 24 cm and a diameter of 0.06 cm. Volumetric flow rate through the fiber is 0.0196 cm^3/sec and the volume fraction of the internal phase is 0.1. The geometry of the model system has been reduced to two-dimensional space for simplicity. The computational domain is a 24 cm $\times$ 0.06 cm rectangle that corresponds to the axial direction, x, and the radial direction, R, in the fiber lumen. Typical diameter of a coarse emulsion droplet is 1 μm. The diameters of droplets in a surfactant-free dispersion of immiscible phase are significantly larger. The drop size of such dispersion is commonly characterized by the Sauter mean diameter. Correlations are available to estimate the Sauter mean diameter by taking into

account the interfacial tension, viscosity, mixing speed, thank and impeller diamters, and phase ratio (11). Typically, the drop diameter is approximately 0.01 cm. If the internal droplets disperse uniformly, the length fraction occupied by the internal phase in each dimension will be $(0.1)^{1/3}$. Thus, there are about 3 droplets ($0.06\times(0.1)^{1/3}\div 0.01=2.78$) in the R direction at any given axial location on average. In the simulation, the internal droplets are introduced into the computational domain at 3 evenly spaced locations along the R direction at the inlet. The velocity profile at the inlet is assumed to be laminar, which is typical in most HFC applications. Specifically, $u = 13.87\text{-}15410.79\times r^2$, where u is the velocity (cm/sec) in the axial direction and r is the radius ($0 \le r \le 0.03$ cm). The velocity of the droplets is assumed to be the same as velocity of the adjacent continuous phase entering the computational domain. At the wall, the no-slip boundary condition is invoked for the continuous phase. The model system uses *n*-tetradecane and a mixture of chlorobenzene and 1-octnol as the continuous phase and 1 N sodium hydroxide as the dispersed phase. Density of *n*-tetradecane, as measured by an Anton Paar DMA 500 Density Meter (Anton Paar, Valparaiso, IN), is 0.765 g/ml. A mixture of 81.62 wt. % chlorobenzene and 18.38 wt. % 1-octanol has a density of 1.040 g/ml, which matches the density of 1N sodium hydroxide solution. The viscosity of *n*-tetradecane was measured to be 1.37 cP using a Fisherbrand calibrated Ubbelohde viscometer. The viscosity of the chlorobenzene mixture is 1.047 cP.

Figure 1 shows the trajectories of water droplets in a water/*n*-tetradecane dispersion. The HFC is horizontally mounted. The arrow right above the x-axis is used as a reference for the velocity vectors and has a magnitude of 50 cm/sec. Due to the density difference between water and *n*-tetradecane, the droplets quickly settle at the bottom of the fiber lumen. Note that the x-axis is reduced by a scale of 0.001 so the figure can have a legible aspect ratio. Although the

velocity vectors point downward only slightly, the trajectories fall rather sharply. Such trajectories suggest that the droplets will accumulate inside the fiber lumen and form slugs eventually, and significantly reduce the contacting area between the solvent and the stripping phase.

Figure 2 shows the trajectories of water droplets in a density-matching, chlorobenzene/*n*-octanol mixture. As expected, the trajectories of the dispersed phase follow the streamlines of the continuous phase. No accumulation of the internal phase is found. Figure 2 was obtained by setting the HFC module horizontally with the gravitation force in the negative R direction. Changes in the mounting direction do not affect the outcome of the simulation. In fact, the exact same figure may be obtained by using a water/*n*-tetradecane mixture (*i.e.* with density differentials) with zero gravitational force. These results suggest that density-matching is a valid way to simulate SFSELM process in the microgravity environment on earth. A result similar to Figure 2 is obtained by using a water/*n*-tetradecane mixture with the HFC module vertically mounted. The magnitude of the velocity vectors of the droplets will be slightly larger but remain on the streamlines of the continuous phase. However, the geometry used in this simulation is extremely simplified. In a real HFC module, the entrance and the exit to the hollow-fiber membrane bundle usually have substantial change in geometry. These changes lead to irregular restriction and expansion of the flow path. Our experimental observations in a similar geometry show that, although the flow remain largely laminar, back-mixing becomes significant when there is a density differential and the streamline and trajectories are no longer straight .

Effect of Coalescence on the Internal Phase Surface Area

The previous section shows that density-matching is a valid way to simulate the microgravity environment on earth. The most critical concern regarding SFSELM extraction however, is whether the design can provide enough stripping capacity for effective extraction, which depends mainly on the coalescence behavior of the internal phase. The breakage and coalescence phenomenon in dispersed two-phase systems has been studied extensively (12,13,14,15). Most studies in the literature concentrate on bubble column reactor or agitated contactors. While many of the theories are applicable to SFSELM, flows in bubble column and agitated contactor are mostly turbulent. On the other hand, flows in hollow-fiber contactor are largely laminar due to the small membrane diameter and slow flow rate. Thus, theories developed for bubble columns and agitated contactors need to be selectively adopted and modified to be applied to SFSELM. In turbulent flow, the energy is frequently strong enough to cause drop breakage, which is unlikely in laminar dispersed flow. Mechanisms that result in drop coalescence in turbulent flows include turbulence, buoyancy, and laminar shear (16). In SFSELM, laminar shear is the only likely mechanism for coalescence, *i.e.*, droplets in faster-moving area catch up with droplets in slower-moving area and coalesce with them. Because the flow is laminar, droplets will not collide due to the macro and micro mixing as in a turbulent flow. Buoyancy is not a concern either because the densities are matched. The coalescence of two droplets takes place in three steps: (1) initial contact of the two drops; (2) drainage and thinning of the liquid film between the two drops; and (3) thickness of the liquid film reduces to a critical level, breakage of the film occurs, and the drops coalesce (12). Step (1) is related to the collision frequency of the drops, ϕ. Collision alone does not guarantee the coalescence of two droplets. Once a collision happens, the drops must remain in contact for a period of time for the

drainage and rupture to occur. Thus, step (2) and (3) may be quantified by a collision "efficiency", ε. The overall coalescence rate, Γ, can then be represented by (16)

$$\Gamma_{mn} = \phi_{mn}\varepsilon_{mn} \tag{8}$$

The subscript m and n denote the sizes of droplets involved in a coalescence event. Simultaneous coalescence between three and more drops is highly unlikely and will not considered here. In this approach, collision events are dictated by the collision frequency, ϕ_{mn}; collision efficiency, ε_{mn}, indicates whether coalescence occurred and is considered independently. The collision frequency from laminar shear may be approximated by (17)

$$\phi_{mn} = \frac{4}{3} N_m N_n \left(r_m^p + r_n^p\right)^3 \frac{-\partial u_x}{\partial R} \tag{9}$$

where $r^p{}_m$ and $r^p{}_n$ are the radii of drops of size m and n, and N_m and N_n are the population densities of drops of size m and n. The collision efficiency, ε_{mn}, may expressed as[14]

$$\varepsilon_{mn} = \exp(-\alpha_{mn}/\beta_{mn}) \tag{10}$$

where α_{mn} is the time required for coalescence, or coalescence time, and β_{mn} is the contacting time between the droplets. The coalescence time can be calculated from[16]

$$\alpha_{mn} = \left(\frac{r_{mn}^3 \rho}{16\sigma}\right)^{1/2} \ln\frac{h_0}{h_f} \tag{11}$$

where σ is the interfacial tension, h_0 is the initial film thickness, h_f is the final film thickness at which film rupture occurs, and the equivalent radius r_{mn} is defined as

$$r_{mn} = \frac{1}{2}\left(\frac{1}{r_m^p} + \frac{1}{r_n^p}\right)^{-1} \tag{12}$$

Contact time in laminar flow is not readily available from the literature but can be easily derived. Consider two droplets, A and B, in a two-dimensional space that depicts the lumen side

of a hollow-fiber membrane as shown in Figure 3. The flow is assumed to be symmetrical in the radial direction and independent of the angular direction in the cylindrical coordinate. The drops, separated by a distance of ΔR in the R direction, are moving in the x-direction at different speeds. The radii of the drops are $r^p{}_m$ and $r^p{}_n$. Collision occurs when $(r^p{}_m+h_0+r^p{}_n)\sin\theta \le \Delta R$ according to the definition from equation (8) to (12), which can be approximated by $(r^p{}_m+r^p{}_n)\sin\theta \le \Delta R$ since h_0 is relatively small. When the two drops collide, the contacting area of both drops will deform, a liquid disk will form between the drops and the draining process begins. As mentioned earlier, if the drops remain in contact long enough, the thickness of the disk will decrease to a critical point, the film will rupture and the two drops merge into a single drop. If the two drops do not coalesce, drop B would have catch up to drop A by a distance of $2(r^p{}_m+r^p{}_n)\cdot\cos\theta \times \beta_{mn}$ during the contact time. Since $\Delta R = (r^p{}_m+r^p{}_n)\cdot\sin\theta$, the contacting time between the two drops is

$$\beta_{mn} = \frac{2\cot\theta}{-\frac{\partial u_x}{\partial R}\left(r_m^p + r_n^p\right)} \tag{13}$$

The contacting time, β_{mn}, will have a value of 0 when θ is 90° ($\Delta R = r^p{}_m+r^p{}_n$) and is infinite when θ is 0 ($\Delta R = 0$). Substituting equation (13) into equation (10); one gets

$$\varepsilon_{mn}(\theta) = \exp\left[-\frac{1}{2}\alpha\left(r_m^p + r_n^p\right)\left(-\frac{\partial u_x}{\partial R}\right)\tan\theta\right] \tag{14}$$

$\varepsilon_{mn}(\theta)$ will have a value of 1 when $\theta = 0$ and is 0 when $\theta = \pi/2$. The average value ε_{mn} may be obtained by

$$\varepsilon_{mn} = \frac{2}{\pi}\int_0^{\pi/2} \varepsilon_{mn}(\theta)\mathrm{d}\theta \tag{15}$$

The integration in equation (15) cannot be easily evaluated analytically. Thus, a numerical method will be employed.

The general trend of coalescence efficiency is shown in Figure 4. The parameter κ may be considered as the combined effect of coalescence time and shear rate. When the value of κ is small, collision is effective from most approaching angles. When κ is large, collision leads to coalescence only when the approaching angle is small. When surfactant is used, the interfacial tension σ in equation (11) is minimized. The time required for droplet coalescence, α_{mn}, becomes extremely large. As a result, the value of κ is large and the collisions become very inefficient. A high shear rate also decreases the collision efficiency by decreasing the contacting time. However, the collision frequency in equation (9) will increase. Another factor that affects the collision efficiency is the drop size; the larger the drops, the less likely that coalescence will occur.

To investigate the coalescence behavior of the droplets, a population balance must be derived for the internal droplets. Consider an organic-aqueous mixture flowing through the lumen side of a hollow fiber membrane. The membrane has an inner diameter of $2R_0$ and a length of L. The flow is assumed to be symmetrical in the radial direction. A tube-shaped, infinitesimal volume inside the fiber lumen can be defined as shown in Figure 5. Flow velocity and droplet size distribution may be considered constant within this infinitesimal volume. The population balance within this volume for a drop of size m may be written as

$$2\pi R(\Delta R)u_x N_m\big|_{x+\Delta x} - 2\pi R(\Delta R)u_x N_m\big|_x = 2\pi R(\Delta R)(\Delta x)\left[\int_0^{m/2}\Gamma_{(m-n)n}\,\mathrm{d}n - \int_0^{\infty}\Gamma_{mn}\,\mathrm{d}n\right] \qquad (16)$$

The first and second terms in equation (16) represent the number of droplets entering and leaving the control volume by convection. The first integration on the right-hand side is the rate of formation of drops of size m by the coalescence of smaller drops per unit volume. The last term accounts for the rate of disappearing of drops of size m due to coalescence. Steady state is assumed so there is no accumulation term in the equation. Equation (16) may be written as an ordinary differential equation

$$\frac{\mathrm{d}N_m}{\mathrm{d}x} = \frac{1}{u_x}\left[\int_0^{m/2}\Gamma_{(m-n)n}\,\mathrm{d}n - \int_0^{\infty}\Gamma_{mn}\,\mathrm{d}n\right] \qquad (17)$$

with a boundary condition of $N_m = N_m{}^0$ at the inlet. Note that N_m, u_x and Γ depend on R as well. Because the flow velocity is zero in the radial direction, the population density in a "tube" as shown in Figure 5 is independent of the population density in an adjacent tube theoretically. The population density at a specific R thus depends only on the axial position x. N_m as a function of x and R can be obtained by integrating equation (17). Once N_m is available, the specific contacting area between the internal phase and the solvent per unit volume may be calculated from

$$A = \frac{2}{R_0^2}\int_0^{R_0} R\cdot\left(\int_0^{\infty} N_m a_m\,\mathrm{d}m\right)\mathrm{d}R \qquad (18)$$

where a_m is the surface area of a droplet of size m. A is a function of x. Velocity profile of a steady-state laminar flow inside a circular pipe is well known (18)

$$u_x = 2u_b\left[1-\left(\frac{R}{R_0}\right)^2\right] \qquad (19)$$

where u_b is the bulk or average flow velocity in the tube.

The simulation is implemented using the Matlab programming language (The MathWorks, Inc., Natick, MA). To simplify the calculation, all drops entering the hollow-fiber membrane are assumed to have the same diameter of 100 μm. At 10% volume ratio, the population density of these drops is 1.91×10^5 drops/cm^3. Population densities of droplets of various sizes along the axial direction are tracked by integrating equation (17). In the last two terms of equation (17), collision events between all possible droplet size combinations must be evaluated. The number of droplet sizes that needs to be tracked increases two fold with each iteration while the number of collision events that needs to be tracked increases exponentially. It is unrealistic to carry out such simulation beyond several iterations. It is obvious that some reasonable assumption needs to be implemented to make such calculations practical. Drops having an N less than 17.7 cm^{-3}, the inverse of the volume of the fiber lumen, are not utilized to calculate subsequent collision events. Because the population density of these drops is already low, the probability that these drops participate in collision events is also low.

Figure 6 shows the typical trend of population density along the axial position. The data were taken at a radial position of 0.0015 cm from the center. Because there is no drop break-up in laminar flow, all drops have a volume proportional to the initial drop volume (size 1). N_1 decays exponentially along the axial direction. Drops of size 2 are formed from the coalescence of two drops of size 1, the dominating event at the entrance of the fiber lumen, and N_2 increases rapidly in this region. As N_2 grows, collision events involving drops of size 2 increases while N_1 keeps decreasing. N_2 starts to decrease about 0.8 cm into the fiber lumen as a result. Similar patterns are observed for drops of size 3 and others; the only difference is that the maximum occurs later and later as the drop size gets larger and larger.

Figure 7 shows that the shear rate has a significant impact on the coalescence rate. The five lines in Figure 7 indicate the changes in N_1 at five different radial position in the tube. A laminar flow in a circular tube has parabolic velocity distribution as indicated by equation (19). The shear rate is zero at the center and reaches the maximum at the wall. As discussed earlier, a high shear rate decreases the contacting time and thus decreases the collision efficiency. On the other hand, high shear rate results in high collision frequency as well. Since coalescence rate is the product of collision rate and collision efficiency, the net effect of high shear rate on the coalescence rate could be either positive or negative. In Figure 7, the closer the drops is to the wall, the faster they coalescence. Such responses suggest that collision rate is the dominating effect on coalescence in this case. A closer inspection reveals that the collision efficiency of drops of size 1 is about 0.995 at all radial position at the entrance. This means when two drops collide, they almost always coalesce. This is mostly due to the high interfacial tension between the internal phase and the solvent. As a result, coalescence rate depends mainly on collision rate and coalescence rate increases as the shear rate increase.

Figure 8 shows the changes in specific contacting area, the contacting area between the solvent and the internal phase per unit volume of mixture, along the axial position. The specific contacting area decreases dramatically after the mixture enters the tube. This is mainly due to the high coalescence rate of drops of size 1. Assuming spherical geometry, several smaller drops always provide larger surface area than a single large drop at the same total volume. The decrease in specific contacting area shown in Figure 8 is even faster than the decrease in population density of drops of size 1 shown in Figure 6. This is because the total surface area is proportional to the square of total drop number. After a few centimeters, the specific contacting area stabilizes at around 12.7 cm^2/cm^3. The average value throughout the fiber lumen is 13.03

cm^2/cm^3. Typical diameter of coarse emulsion droplet is about 1 μm. At a volume fraction (internal phase/emulsion) of 0.1, there will be 1.91×10^{11} droplets per milliliter of emulsion, which provide a specific contacting area of 6000 cm^2/cm^3. This number is significantly larger than the 13.03 cm^2/cm^3 obtained from SFSELM. On the other hand, without taking porosity in to account, the fiber lumen provides a specific contacting area of only 66.7 cm^2/cm^3. Once the porosity is taken into account, the specific area provided by the hollow-fiber membrane should be comparable or less than that provided by SFSELM because extraction can only happen at the pore openings. The thickness of the hollow-fiber membrane is also significantly larger than the thickness of the boundary layer surrounding the stripping phase droplets. In addition, the partition coefficient in the extraction step is typically low due to toxicity considerations when selecting the solvent (7). The stripping step, on the other hand, always has a partition coefficient that highly favors the stripping phase. All these factors will contribute to the overall mass transfer resistance in the hollow-fiber membrane. Thus, the stripping process in the SFSELM design is unlikely to become a rate-limiting step of the extraction process. In the worst case scenario, the SFSELM design simply becomes the same as the supported liquid membrane (SLM) design (19). However, loss of solvent due to its solubility in water is a major concern in SLM extraction.20 The SFSELM design will not have this problem because the solvent is constantly replenished to the membrane pores. In short, SFSELM is a feasible way to conduct solvent extraction with simultaneous stripping for extraction tasks in the microgravity environment.

Summary

The feasibility of SFSELM extraction was assessed in this research. SFSELM extraction was conceived as a mean to conduct extractive fermentation in the microgravity environment. Due to the absence of the gravitational force, a stable water-in-oil dispersion can be maintained without the use of surfactant. Such a design preserves the advantages of SELM extraction, namely eliminating the equilibrium constraint of solvent extraction and stable operation, while simplifying the product recovery process because no demulsification is necessary. Trajectories of the dispersed phase in a SFSELM flow was studied using the Lagrangian method. Effects of density differential between the two phases, HFC module orientation, and gravitational force were examined. It was found that matching the density of the two phases has the same effect of zero gravity. The result suggests that SFSELM extraction in the microgravity environment can be simulated by matching the density of the internal phase and the solvent. One shortcoming of SFSELM is the reduced contacting area between the solvent and the internal phase, which may limit the stripping efficiency. In addition, drop coalescence becomes a significant phenomenon because the interfacial tension is no longer minimized without surfactant. In a SFSELM flow, the main mechanism of drop coalescence is laminar shear, *i.e.* drops in the faster-flowing region catch up to drops in the slower flowing region and collide. The coalescence phenomenon is studied by taking into account of collision frequency and collision efficiency. It was found that, without surfactant, the collision efficiency is nearly 100% in a typical SFSELM flow. Collision frequency is the dominant effect that determines the coalescence rate. Coalescence is most prominent in regions where velocity gradient is large, such as near the wall in a laminar flow. Nevertheless, the contacting area between the internal phase and the solvent is comparable to the area for extraction offered by the hollow-fiber membrane. Thus, the SFSELM design should be

able to sustain the stripping process, providing an efficient way to conduct solvent extraction and simplifying the downstream product recovery process i the microgravity environment.

Acknowledgement

The authors would like to thank NASA for the funding of this project.

List of Symbols

A	Specific contacting area between the solvent and the internal phase, cm^2/cm^3
a	Surface area of a single internal phase droplet
C_D	Drag coefficient
D	Particle or drop diameter, cm
E	Designate a control volume of interest
g	Gravitational acceleration, cm/s^2
h_0, h_f	Initial and final film thickness during coalescence, cm
L	Fiber length
n	Number of droplets
N	Population density of the internal phase droplets, $1/cm^3$
p	Pressure, $dyne/cm^2$
R	Radial direction within the membrane lumen, cm
r	Radius of an internal phase droplet
R_0	Radius of the fiber lumen, cm
Re	Reynolds number
r_{mn}	Equivalent radius, cm
t	Time, s
u	Flow or particle velocity, cm/s
V	Volume, cm^3
x	Axial direction inside the fiber lumen, cm
x_j	x_1, x_2, x_3, represent x, y and z respectively, cm

Greek Letters

Φ	Source term in the governing equations; Φ^m is the mass source (g/cm^3 s) and Φ^M is the momentum source ($dyne/cm^3$)
Γ	Coalescence rate, $1/cm^3 \cdot s$
α	Coalescence time, s
β	Contacting time, s
δt	Residence time of droplets within a control volume
ε	Collision efficiency
ϕ	Collision frequency, $1/cm^3 \cdot s$
η	Number of droplets within a control volume
κ	Combined effect of coalescence time and shear rate
λ	Particle relaxation time, s
μ	Viscosity, g/cm·s
θ	Approaching angle during drop collisions
ρ	Density, g/cm^3

σ Interfacial tension, dyne/cm^2

τ Normal and shear stress, dyne/cm^2

Superscripts and Subscripts

b Bulk or average property inside the fiber lumen

E Property within the control volume *E*

i, j Direction in the Cartesian coordinate; *i* or *j* = 1, 2 and 3 corresponds to the X,Y and Z direction respectively.

k Property of a specific drop trajectory

m, n Designate drop of certain sizes. Analytically, *m* and *n* can range from 0 to infinite. In the numerical simulation, m and n represent how many times a drop is larger than drops at the entrance All drops at the entrance have a size of 1. *m* = 121, for example means a drop is 121 time larger volume-wise than the drops at the entrance

p Property of an internal phase droplet

References

1 Hu, S B. and Wiencek, J. M., *AIChE J.* **44**, 570, 1998.

2 Breembroek, G. R. M., van Straalen, A., Witkamp, G. J. and van Rosmalen, G. M., *J. Membr. Sci.* **146**, 185, 1998.

3 Nanoti, A., Ganguly, S. K., Goswami, A. N. and Rawat, B. S., *Ind. Eng. Chem. Res.* **36**, 4369, 1997.

4 Lissant, K., Demulsification - Industrial Applications, in *Surfactant Science Series, Vol. 13* , 1992.

5J. Draxler, J., Furst, W. and Marr, R., Separation of Metal Species by Emulsion Liquid Membrane, *J. Membr. Sci.* **38**, 281, 1988.

6 Tirmizi, N. P., Raghuraman, B. and Wiencek, J., Demulsification of water/oil/solid emulsions by hollow-fiber membranes, *AIChE J.* **42**, 1263, 1996.

7 Li, J., Hu, S. B. and Wiencek, J. M., Development of a Supported Emulsion Liquid Membrane System for Propionic Acid Separation in a Microgravity Environment, *Biotechnol. Bioprocess Eng.* **6**, 4261, 2001.

8 Anderson, T. B. and Jackson, R., A fluid dynamical description of fluidized beds, *Ind. Eng. Chem. Fundam.* **6**, 527, 1967.

9 Manninen, M , Taivassalo, V. and Kallio, S., On the Mixture Model for Multiphase Flow, VIT Publications, Technical Research Centre of Finland , 1996.

10 Migdal, D. and Agosta, D., A Source Flow Model for Continuum Gas-Particle Flow, *Trans. ASME, J. Appl. Mech.* **34E**, , 1967.

11 Skelland, A. and Lee, J., Drop Size and Continuous-Phase Mass Transfer in Agitated Vessels, *AIChE J.* **27**, 99, 1981.

12 Valentas, K. J. and Amundson, N. R., Breakage and Coalescence in Dispersed Phase Systems, *I&EC Fund* **5**, 533, 1966.

13 Kirkpatrick, R. D. and Lockett, M., The Influence of Approach Velocity on Bubble Coalescence, *Chem. Eng. Sci.* **29**, 2363, 1974.

14 Coulaloglou, C. and Tavlarides, L. L., Description of Interaction Processes in Agitated Liquid-Liquid Dispersions, *Chem. Eng. Sci* **32**, 1289, 1977

15 Millies, M. and Mewes, D., Interfacial area density in bubbly flow, *Chem. Eng Process.* **38**, 307, 1999.

16 Prince, M. J. and Blanch, H. W., Bubble Coalescence and Break-Up in Air-Sparged Bubble Columns, *AIChE J.* **36**, 1485, 1990

17 Friedlander, S. K., in *Smoke, Dust, and Haze, 2nd Ed.*, pp.200, 2000.

18 Bird, R. B., Stewart, W. E. and Lightfoot, E. N., *Transport Phenomena*, John Wiley & Son , 1960.

19 Ward, W. J. and Robb, W. L., Carbon Dioxide-Oxygen Separation: Facilitated Transport of Carbon Dioxide across a Liquid Film, *Science* **156**, 1481, 1967.

20 Danesi, P. R., Yinger, R. and Rickert, P. G., Lifetime of Supported Liquid Membranes: The Influence of Interfacial Properties, Chemical Composition and Water Transport on the Long-Term Stability of the Membrane, *J. Membr. Sci,* **31**, 117, 1987.

Figure Captions

Figure 1. Trajectories of water droplets in *n*-tetradecane in a horizontally mounted HFC.

Figure 2. Trajectory of water droplets in a density-matching mixture.

Figure 3. Derive contacting time between droplets in laminar flow.

Figure 4. Effect of coalescence time and shear rate on collision efficiency.

Figure 5. An infinitesimal, tube-shaped geometry in the fiber lumen is used for population balance of the internal phase.

Figure 6. Population densities of drops of size 1, 2 and 3 at a radius of 0.0015 cm.

Figure 7. Population densities of drop of size 1 at various axial and radial positions.

Figure 8. Specific contacting area between solvent and the internal phase in SFSELM

Figure 1. Trajectories of water droplets in *n*-tetradecane in a horizontally mounted HFC.

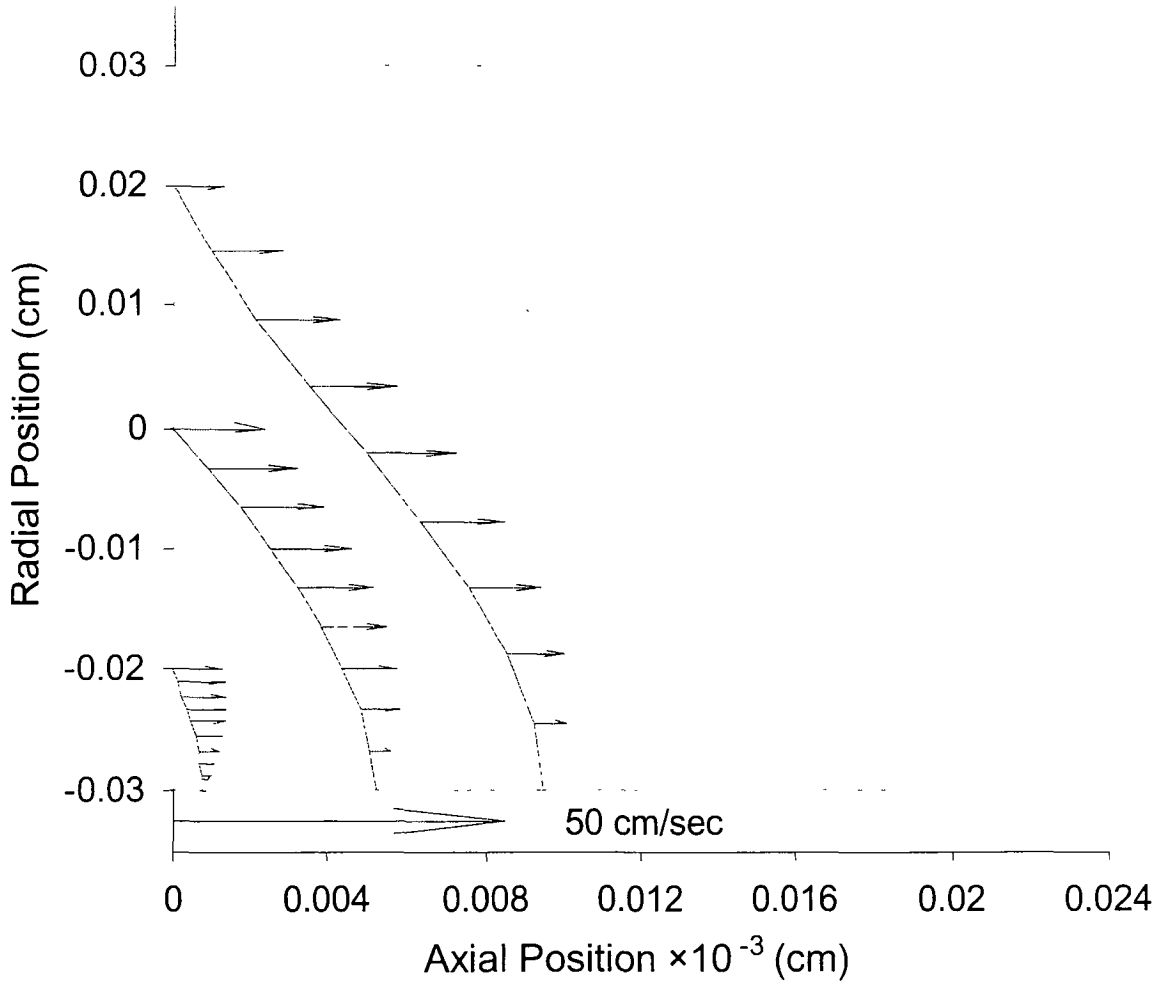

Figure 2. Trajectory of water droplets in a density-matching mixture.

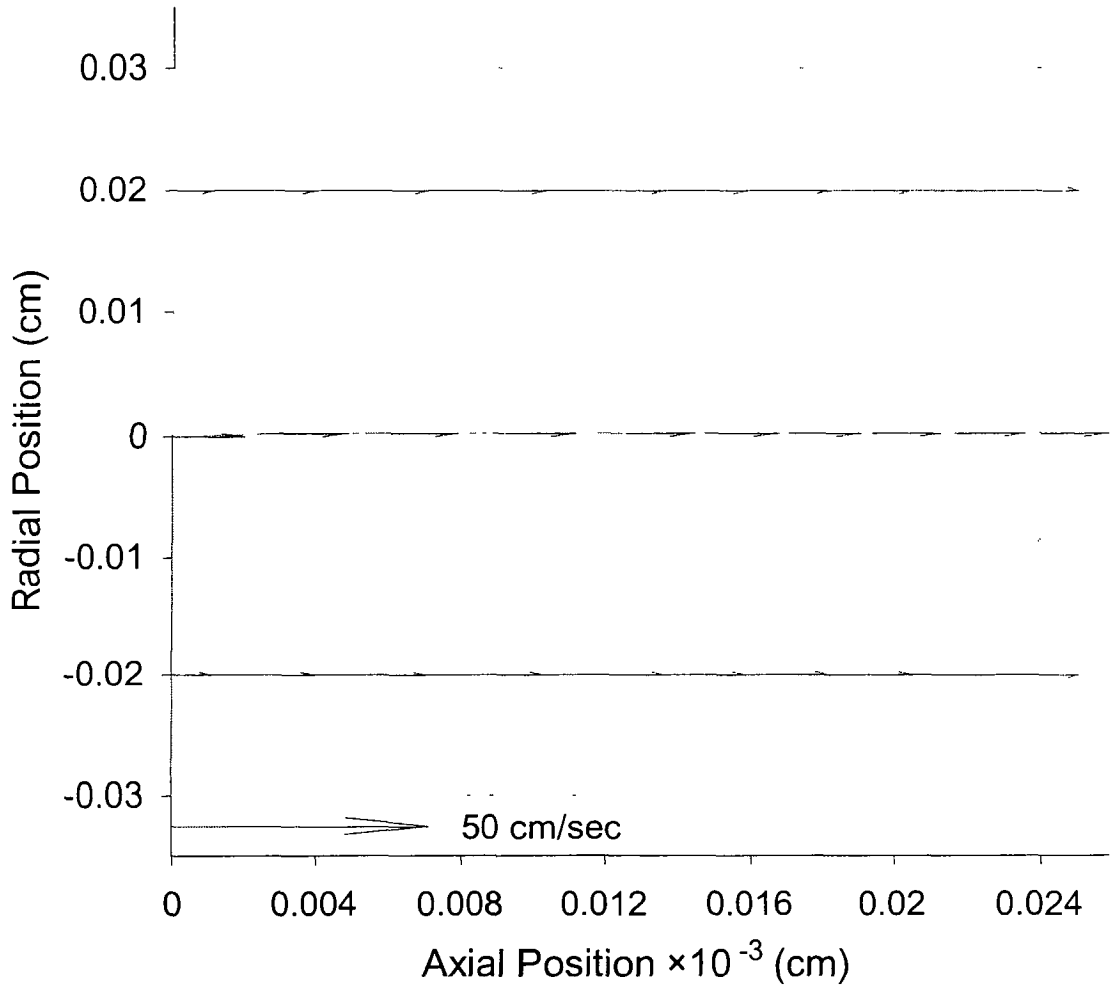

Figure 3. Derive contacting time between droplets in laminar flow.

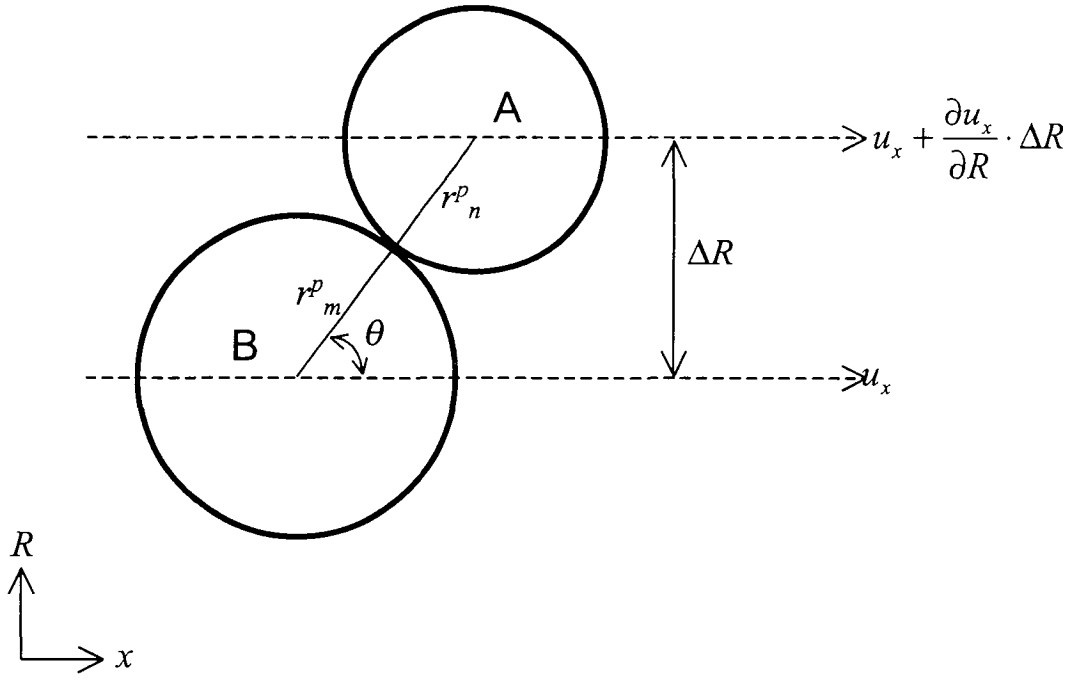

Figure 4. Effect of coalescence time and shear rate on collision efficiency.

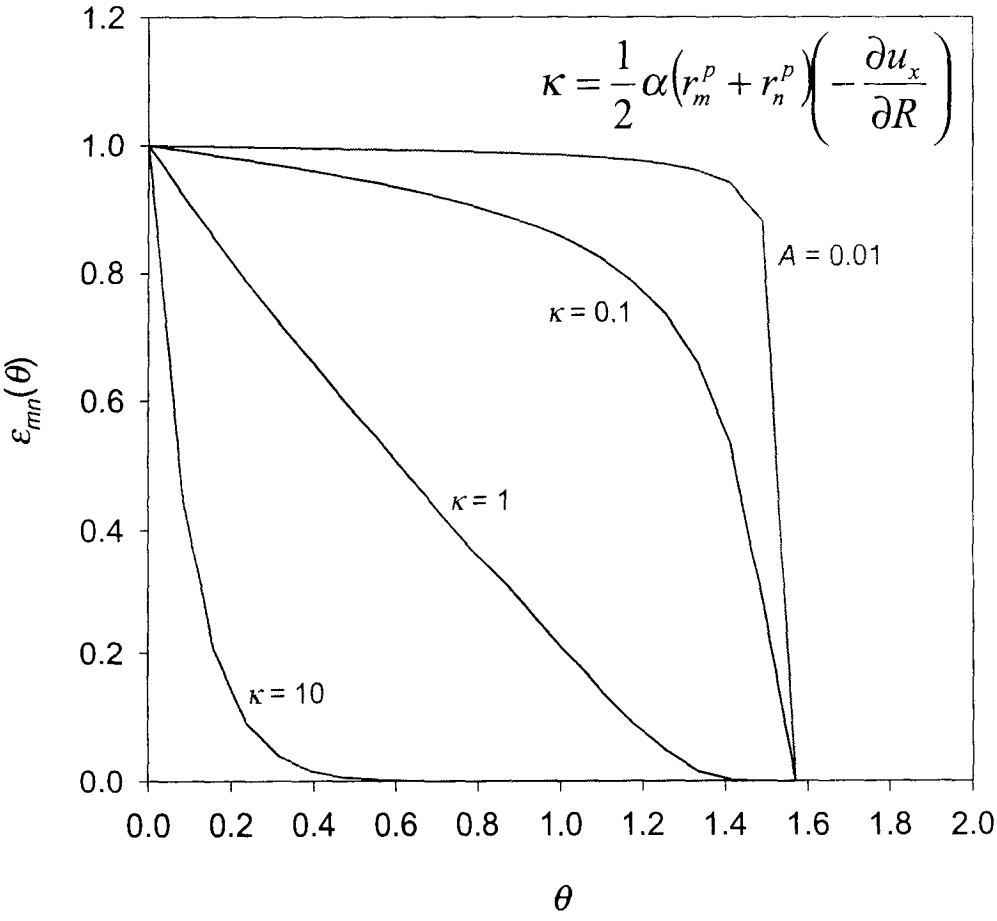

Figure 5. An infinitesimal, tube-shaped geometry in the fiber lumen is used for population balance of the internal phase.

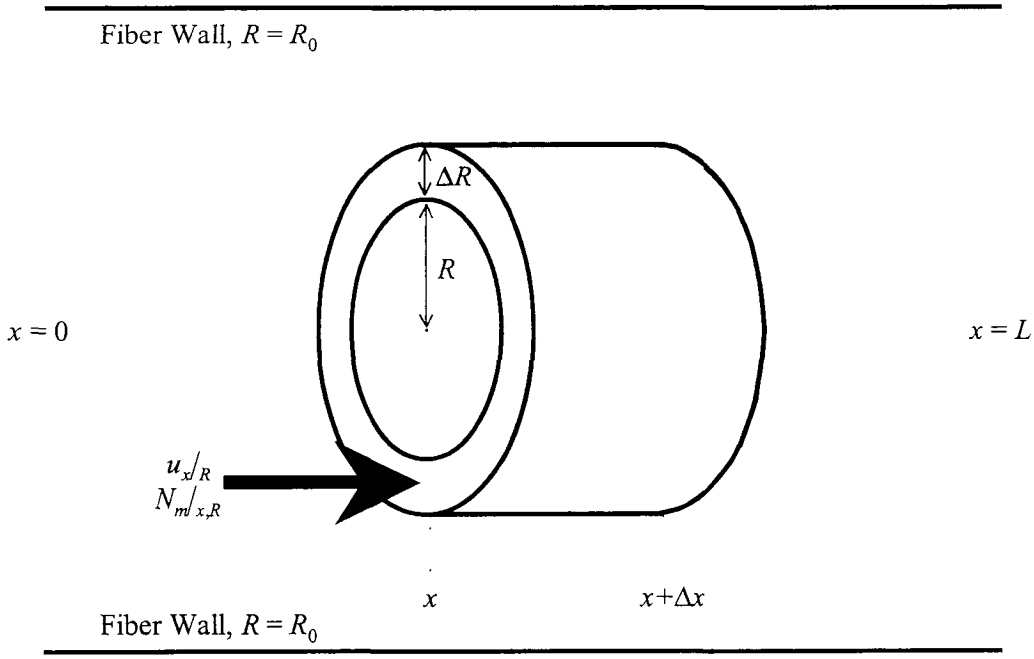

Figure 6. Population densities of drops of size 1, 2 and 3 at a radius of 0.0015 cm.

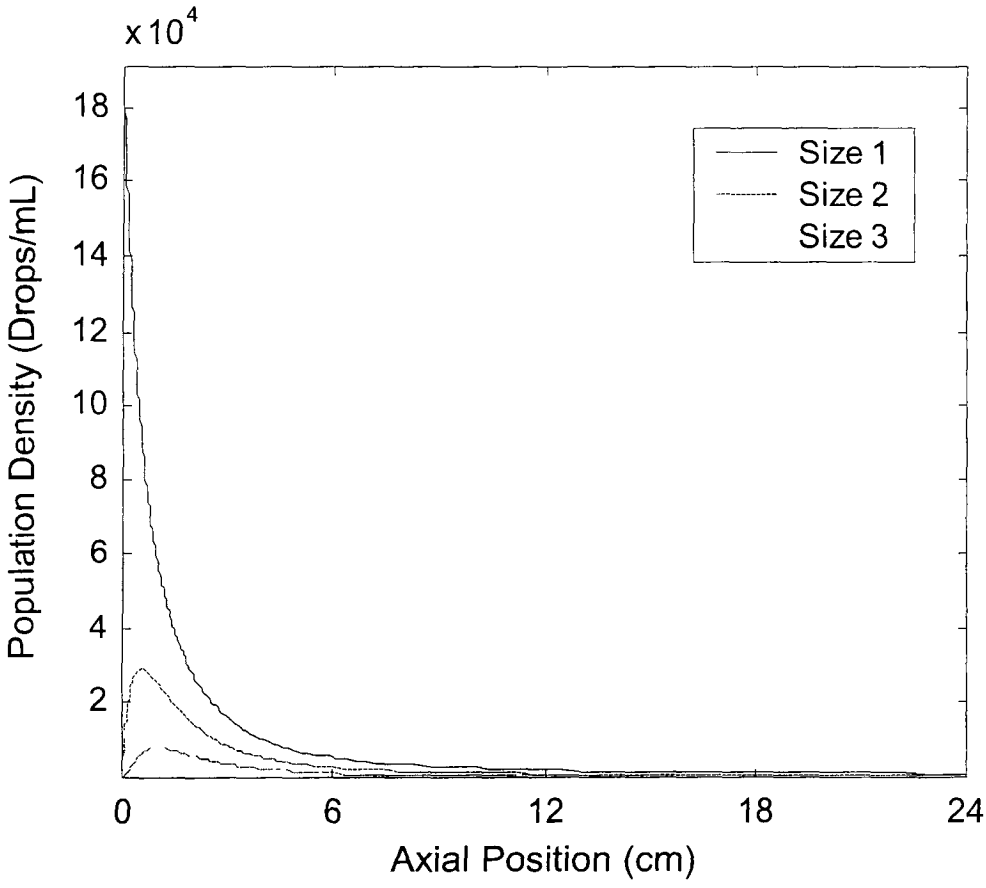

Figure 7. Population densities of drop of size 1 at various axial and radial positions.

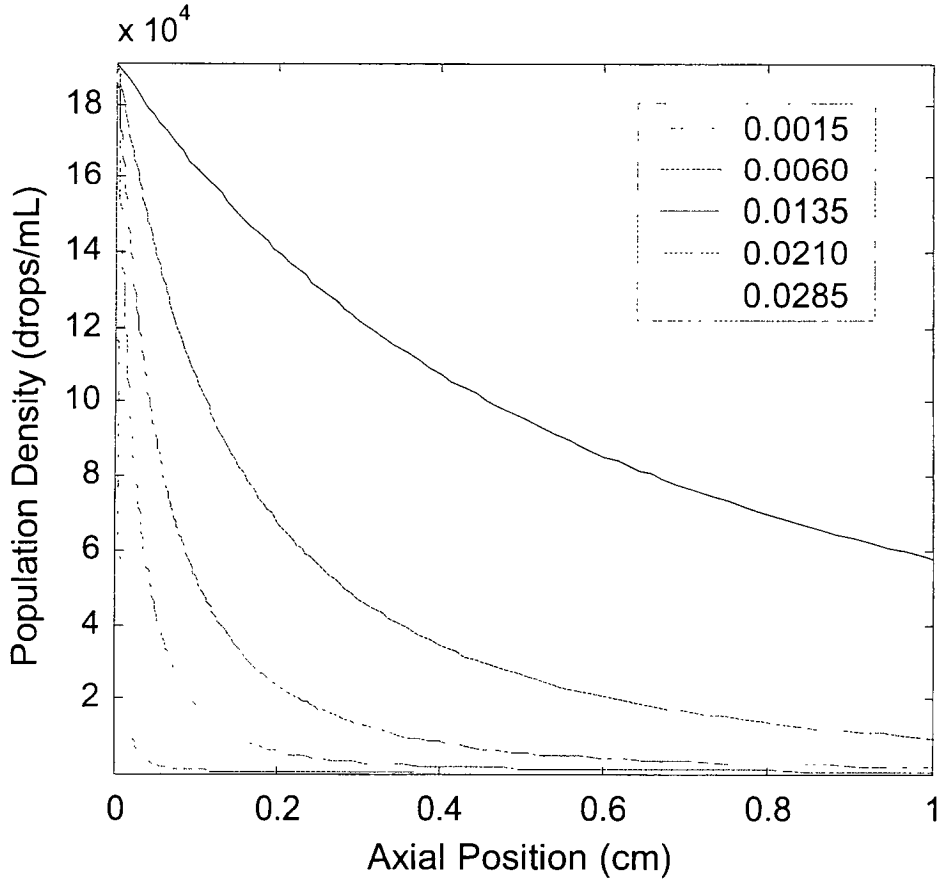

Figure 8. Specific contacting area between solvent and the internal phase in SFSELM